INSTITUTE OF PHYSICS PUBLISHING PLASMA SOURCES SCIENCE AND TECHNOLOGY
Plasma Sources Sci. Technol. **14** (2005) 581–588 doi:10.1088/0963-0252/14/3/022

# Two-dimensional ion velocity distribution functions in inductively coupled argon plasma

**David C Zimmerman**[1,4], **Roger McWilliams**[2] **and David A Edrich**[3]

[1] The Optical Sciences Company, Anaheim, CA 92806, USA
[2] Department of Physics and Astronomy, University of California at Irvine, Irvine, CA 92697, USA
[3] Scientific Applications and Research Associates Inc., Cypress, CA 90630, USA

Received 17 February 2005, in final form 29 May 2005
Published 27 June 2005
Online at stacks.iop.org/PSST/14/581

**Abstract**
Two-dimensional ion velocity distribution functions (IVDFs) of argon plasmas have been measured with optical tomography via laser-induced fluorescence (LIF). An inductive radio-frequency (RF) coil created the plasmas, and IVDFs were measured versus RF frequency, gas pressure and location (bulk plasma or presheath of a plate). Typical gas pressure was 0.3–0.4 mTorr, RF power 25 W and magnetic field 130 G. Effective perpendicular ion temperature decreased with increasing RF frequency, and changed little with pressure. Optical tomography reveals features of the presheath IVDF that cannot be deduced from LIF scans parallel and perpendicular to the plate alone. Progress also has been made toward performing optical tomography on a commercial ion beam source (Veeco/Ion Tech 3 cm RF Ion Source, Model #201). In particular, it has been discovered that the beam energy fluctuates in a range of about 20 eV over the timescale of a few minutes.

## 1. Introduction

Knowledge of the velocity distribution of plasma is important in plasma processing applications. Increasing surface feature precision places ever-tighter constraints on the processing plasma distribution function (and the moments of convective flow, temperature, etc). For example, control of the ion impact angle relative to the surface normal allows some control of the angle of etched trench sidewalls. Many plasma processing applications involve inductively coupled radio-frequency (RF) plasma sources. This paper examines the velocity distributions of plasmas created by inductive RF plasma sources using laser-induced fluorescence (LIF) in argon, both in bulk plasma, and in the presheath near a plate. Optical tomography allows a reconstruction of the 2D or 3D velocity distribution from a series of 1D LIF scans, revealing velocity space structure that cannot be seen in the 1D scans.

Much work has been done in advancing the science and technique of LIF and optical tomography to its current state. Koslover *et al* [1] worked together to develop, refine [2] and apply [2–4] the technique and apparatus for performing optical tomography. Scime *et al* [5] and Biloiu *et al* [6] have also developed optical tomography apparatus. The development of diode lasers [7] allowed the use of less expensive lasers (compared to dye lasers) in this work. This work described here builds on the foundation of the previous work on argon plasma LIF. Edrich *et al* [8] have studied ion diffusion and scattering using LIF. Sadeghi *et al* [9] have also studied ion transport. Giapis *et al* [10] have studied the effects of metastable ions on surface energy flux. Brockhaus *et al* [11] determined the beam velocity of an ion beam source similar to the one used in this study.

## 2. Theory

### 2.1. Ion–neutral collisions

The mean free path of an ion in its neutral gas is roughly inversely proportional to gas density, the relation being (with temperature held constant)

$$\lambda = \frac{1}{n\sigma} = \frac{kT}{P\sigma} = \frac{1}{3.218 P_{\mathrm{Torr}} \sigma \text{ Å}^2}\text{cm}, \qquad (1)$$

where $\lambda$ is the ion's mean free path, $k$ is Boltzmann's constant, $T$ is the gas temperature, $P$ is the gas pressure and $\sigma$ is the total

[4] Author to whom any correspondence should be addressed. Present address: The Optical Sciences Company, PO Box 25309, Anaheim, CA 92825-5309, USA.

ion–neutral collision cross-section, which can be dependent on pressure, ion velocity and other parameters. For the numerical formula, the gas temperature is assumed to be 300 K. Using an argon ion–neutral collision cross-section of 140 Å$^2$ [12] at a pressure of $3.5 \times 10^{-4}$ Torr, $\lambda = 6.3$ cm. This cross-section is used because $T_{\mathrm{ion}} \gg T_{\mathrm{gas}}$. For slow ions ($v_{\mathrm{ion}} \leqslant v_{\mathrm{gas}}$), the collision cross-section is 200 Å$^2$ [12], giving $\lambda = 4.4$ cm at the same pressure. Usually, the distance from the plasma source to the measurement point was much larger than $\lambda$, in which case the diagnostic measured ions that had undergone many collisions. Note that these cross-sections are difficult to determine, and are therefore estimates whose applicability to the prevailing experimental conditions is uncertain.

### 2.2. Ion–RF field interactions

RF plasma is created and sustained by the interaction between the RF field and plasma electrons; however, the plasma ions interact with the RF field also. In the case of inductive plasma sources, an axial magnetic field with sinusoidal time dependence exists due to the current flowing through the inductive-source solenoid. This magnetic field induces an electric field by Faraday's law,

$$\frac{\partial \vec{B}}{\partial t} = -\nabla \times \vec{E}. \tag{2}$$

The resulting electric field is in the azimuthal direction, sinusoidally varying in time as the magnetic field, but out of phase by $\pi/2$ rad. This electric field accelerates the ions normal to the coil axis, which results in a higher effective temperature in that direction. The effective temperature of the ions should be understood in the following way: the LIF measurements were much slower than the RF frequency, so the average number of ions at each velocity over an RF cycle was measured, i.e.

$$f(v) = \frac{\omega}{2\pi} \int_0^{2\pi/\omega} f(v,t)\mathrm{d}t, \tag{3}$$

where $\omega$ is the RF angular frequency and $f(v,t)$ is the instantaneous ion velocity distribution. The effective temperature measured from $f(v)$ is a superposition of the true thermodynamic temperature of $f(v,t)$ and coherent motion of ions in the RF field. This effective temperature is important to plasma processing because when ions strike a surface, motion parallel to the surface can cause undesired effects such as undercutting in trenches, and this parallel motion arises from both thermodynamic temperature and the 'sloshing' back and forth of ions in the electric field. In the rest of this paper, the term 'temperature' refers to the effective temperature unless otherwise specified.

The background magnetic field in the experiments done here was so small that $f_{\mathrm{RF}} \approx 10\,000 f_{\mathrm{ci}}$, so that cyclotron effects were ignored.

### 2.3. Plasma sheath and presheath

The width of the sheath typically is of the order of a few Debye lengths [13], and the width of the presheath is of the order of the ion–neutral collision mean free path [13, 14]. As stated above, the ion–neutral collision mean free path is about 6 cm in the present experiments, and the Debye length can be calculated from the equation

$$\lambda_{\mathrm{D}} = \sqrt{\frac{\varepsilon_0 k T_{\mathrm{e}}}{n e^2}}, \tag{4}$$

where $\varepsilon_0$ is the permittivity of free space, $k$ is Boltzmann's constant, $T_{\mathrm{e}}$ is the electron temperature, $n$ is the plasma density and $e$ is the electronic charge. Using typical experimental conditions as measured by a Langmuir probe ($T_{\mathrm{e}} = 8$ eV, $n = 10^{10}$ cm$^{-3}$, gas pressure $= 0.35$ mTorr), the Debye length is 0.02 cm. The Langmuir probe was not RF-compensated.

### 2.4. Laser-induced fluorescence

A narrowband laser beam excites metastable atoms or ions satisfying the condition

$$\omega_{\mathrm{laser}} = \omega_0 + \vec{k} \cdot \vec{v}, \tag{5}$$

where $\omega_{\mathrm{laser}}$ is the angular frequency of the laser, $\omega_0$ is the nominal angular frequency of the transition, $\vec{k}$ is the wavevector of the laser photon and $\vec{v}$ is the velocity of the ion. In the direction of $\vec{k}$, this equation is equivalent to the relativistic Doppler shift condition,

$$v = \frac{c\Delta f}{f_0 + \Delta f} \approx \frac{c\Delta f}{f_0} = \lambda_0 \Delta f, \tag{6}$$

where $v$ is the ion speed, $c$ is the speed of light, $f_0$ is the nominal transition frequency, $\Delta f$ is the difference between the photon's frequency and $f_0$, and $\lambda_0$ is the nominal transition wavelength. The approximation is valid because $f_0$ is around $10^{14}$ Hz and $\Delta f$ is around $10^9$–$10^{10}$ Hz. Once an ion is excited, it may relax to a different state, and the photons emitted during this transition are observed.

### 2.5. Optical tomography

A single LIF scan is a projection of the 3D ion velocity distribution function (IVDF) in the direction of $\vec{k}$. For a scan with the laser at an angle $\theta$, the projected velocity distribution is

$$f_\theta(v_{\mathrm{s}}) = \int_{-\infty}^{\infty}\int_{-\infty}^{\infty} f(v_x, v_z)\delta[v_{\mathrm{s}} - (v_x \cos\theta + v_z \sin\theta)]\mathrm{d}v_x \mathrm{d}v_z. \tag{7}$$

The reverse process, known as filtered back-projection, recreates the 2D IVDF from a series of 1D projections taken at different angles within a plane. If the projections at all angles are known, the 2D IVDF can be reconstructed perfectly according to the formula

$$f(v_x, v_z) = \frac{1}{2\pi}\int_0^{\pi} \mathrm{d}\theta \int_{-\infty}^{\infty} F^{-1}[F[f_\theta(v_{\mathrm{s}})] \cdot |k_v|] \times \delta(v_x \cos\theta + v_z \sin\theta - v_{\mathrm{s}})\,\mathrm{d}v_{\mathrm{s}}, \tag{8}$$

where $F$ represents a Fourier transform and $k_v$ is the conjugate variable to $v_{\mathrm{s}}$. If a finite number of projections at constant angle increments over the range $[0, \pi)$ are known, the formula becomes

$$f(v_x, v_z) \approx \frac{1}{2N}\sum_{n=1}^{N} F^{-1}\left[F\left[f_n\left(v_x \cos\frac{n-1}{N}\pi + v_z \sin\frac{n-1}{N}\pi\right)\right] \cdot |k_v|\right], \tag{9}$$

where $N$ is the number of projections, and it is implied that $f_n$ is evaluated after performing the Fourier transforms. A finite number of scans limits the resolution of the reconstruction according to the relation

$$\frac{\delta v}{v} = \frac{\pi}{2N}, \tag{10}$$

where $\delta v$ is the minimum resolvable feature size and $v$ is the scan width. Features smaller than $\delta v$ will be smeared out [2]. For 12 scans (15° per scan), this resolution is 13% of the scan width, and for 18 scans (10° per scan), the resolution is 9%.

### 2.6. Zeeman splitting

A magnetic field splits degenerate atomic energy levels with different $z$-components of orbital angular momentum in what is known as the Zeeman effect. This split is proportional to the square of the strength of the magnetic field and causes atomic transition lines to broaden. For the magnetic field strengths considered here, the Zeeman effect adds about $10^{-3}$ eV of temperature to the LIF measurements and is ignored. The experiments were conducted with a small magnetic field to avoid complications arising from the Zeeman effect.

## 3. Experimental set-up

### 3.1. Vacuum vessel and magnetic field

The experiments were performed in a cylindrical vacuum vessel with a mildly-mirrored magnetic field configuration. In the optical tomography experiments, the magnetic field varied from 50 G at the plasma source to 130 G at the LIF measurement point. The magnetic field for the ion beam experiments was 200 G.

### 3.2. Plasma sources

The main plasma source used in this study was simply six turns of copper wire, the resulting solenoid having a diameter of 3.8 cm and a length of 5.6 cm. It was contained in an open-ended cylindrical metal shell with a diameter of 7.4 cm and a length of 10.2 cm. One end of the coil was attached to the shell which was grounded, and the other attached to the RF through a capacitive matching network. The axis of the coil lay roughly along the axis of the vessel and magnetic field; tilting the source varied the amount of light that the plasma emitted, so some experiments were done with the source slightly tilted to maximize the emitted light. The matching network provides a resonance of about 18.5 MHz, and another resonance exists around 100 MHz. Both resonances were used in this study. The plasma created by this source was concentrated in a column of approximately the diameter of the source, although the plasma filled the entire vessel. The distance from the coil to the LIF measurement point was 45 cm.

The ion beam source is a commercially available Veeco/Ion Tech 3 cm RF Ion Source, Model #201 (see figure 1). The source is modified [15] from stock form for use in related experiments. For charge neutralization, the source requires electrons to be available externally, produced in this case by a hot tungsten filament. The frequency of the RF power applied to the ion beam source was approximately 18.5 MHz.

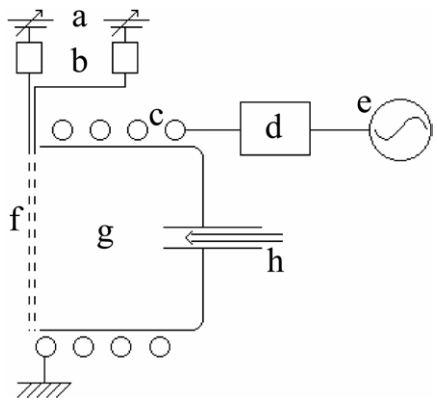


**Figure 1.** Ion beam source: (a) dc power supplies, (b) low-pass filters, (c) RF coil, (d ) capacitive matching network, (e) RF generator and amplifier, (f) grids, (g) plasma discharge contained in quartz cup, (h) gas feed and inflowing argon.

A positive potential on the screen grid raises the potential of the plasma in the cup. The accelerator grid is biased negative with respect to the screen grid. Therefore, any plasma that drifts from the cup into the region between the grids will be separated, the ions leaving the source and the electrons being collected by the screen or re-entering the cup. Varying the voltage difference between the screen and accelerator grids will therefore vary the energy of the ion beam. The vacuum feedthrough of the source allows rotational and radial motion.

### 3.3. Plate

In the optical tomography experiments, a sheet of aluminium foil served as a plate and created the presheath in which LIF measurements were made. The plate was normal to the magnetic field and mounted on a probe shaft to allow the plate to be withdrawn as needed. The plate was biased about 75 V below the ground to attract ions and repel electrons; however, the presheath IVDF varied little as a function of plate bias.

### 3.4. Optics

A New Focus Vortex external-cavity diode laser with 6 mW of single mode 6686 Å light seeded an SDL-8630 laser diode, which amplified the light up to 65 mW [4]. The seed laser is tunable over 100 GHz, and interfaced with the computer controlling the experiment via GPIB. The frequency steps of the seed laser are almost constant over the course of a scan. Light from the seed laser passed through an optical isolator and polarization rotator to protect the seed laser. The light then entered the single-pass amplifier, where the master oscillator power amplifier (MOPA) amplified the laser light. The light then passed through another optical isolator to protect the MOPA (experience shows that any amplified light returning to the MOPA will cause it to burn up), an iodine cell for an absolute wavelength reference and a Stanford Research Systems model SR540 chopper for modulation at 4 kHz to enable the use of a lock-in amplifier. The wavelength of the laser light was determined by passing it through a cell filled with gaseous iodine and using the known fluorescence lines of iodine [16].

For measurements not requiring spatial resolution, a 2″ diameter photomultiplier tube (PMT) with a 10 Å, 3° acceptance angle filter centred on 442.6 nm collected light from the plasma. The PMT was kept at least 30 cm outside of the magnetic field coils to minimize the effect of the magnetic field on the operation of the PMT. When spatial resolution was needed, additional optics were used. A 7 cm focal length lens placed 14 cm from the laser line focused the collected light onto a 1 mm diameter fibre optic cable 14 cm from the lens. A collimator at the end of the fibre optic cable directed the light from the plasma through the filter and into the PMT. This system [8] has a resolution of 2 mm, but it reduces the LIF signal by a factor of 1000, and the signal-to-noise ratio is lower.

### 3.5. Optical tomography

Rotation of the laser beam $\vec{k}$ through $\theta$ ($\pm$ 2°) was achieved by means of a tomography hook [2, 3]. A fibre optic cable passes through a 3/8″ ($\approx$1 cm) stainless steel rod bent into a hook shape, with a focusing lens on the end. The hook focuses laser light to a minimum diameter of approximately 4 mm at the rotation axis of the hook, facilitating optical tomography at the focal point. A 6″ flange mounts the hook to the vacuum vessel. The feedthrough of the hook allows radial and rotational motion. The hook is coated with an insulating material so that its effect on the plasma potential field is minimal.

The design of the hook is such that it does not disturb the plasma at the measurement point. For the current experimental conditions, the hook did not disturb the plasma at the observation point even when rotated such that it lay directly between the plasma source and measurement point, which was necessary since the measurement point was only a few centimeters or less away from the plate. The distance from the focusing lens to the measurement point was 5 cm. The hook tube diameter was much less than an ion Larmor radius in most cases. This combination of geometries meant that no perturbation due to the hook would be expected at the observation point. This was verified experimentally in that the LIF data were very similar for small changes in angle where the hook began to block the line of sight from the source to the observation point.

When taking tomographs of plasma in the presheath, the full suite of collection optics was required, since spatial resolution, i.e. distance from the plate, was important. On the other hand, when taking tomographs of background plasma, only the filter and PMT were needed, which allowed for faster, less noisy scans.

## 4. Optical tomography: results and discussion

Optical tomography was performed with the RF coil source under various conditions. The RF coil source creates plasma and metastable ions throughout the vacuum vessel. Therefore, the strength of the LIF signal generally increases with gas density (plasma and metastable density increase). However, the mean free path for ion–neutral collisions is inversely proportional to gas density, presenting a trade-off condition. The goal of a given experiment determines the optimum gas density/pressure for that experiment. In the case of optical tomography, temperature anisotropy and ion drift velocities were of prime interest, so a long mean-free path was desired—a short mean-free path would lead to excessive collisional damping of temperature and drift. LIF signal strength was sacrificed to produce less collisional plasmas by operating at low pressures.

**Table 1.** Experimental parameters for the optical tomography experiments with column headings corresponding to figure 2.

| | *a* | *b* | *c* | *d* | *e* |
|---|---|---|---|---|---|
| RF frequency (MHz) | 18.62 | 106.5 | 18.81 | 18.62 | 106.5 |
| Radiated RF power (W) | 23.0 | 26.0 | 31.8 | 25.3 | 26.1 |
| Gas pressure ($10^{-4}$ Torr) | 3.3 | 3.2 | 1.4 | 3.5 | 3.9 |

The coordinate system used is as follows: the $z$ axis is in the axial direction (parallel to the symmetry axis of the vessel and the background magnetic field axis, positive toward the plate), the $x$ axis is in the vertical direction (perpendicular to the symmetry axis of the vessel), and $\phi$ is the angle of the laser beam from the $z$ axis in the $xz$ plane. The RF coil and LIF detection point were slightly off-centre from the vacuum vessel axis.

The results of the optical tomography study are given below. The velocity distributions vary in temperature with the RF frequency. Background gas density does not significantly affect the distribution in the explored pressure range. The presence of a plate significantly alters the distribution. See table 1 for a summary of experimental conditions. The magnetic fields at the RF source and LIF point were typically 90 G and 130 G, respectively.

The tomographs (figure 2) are displayed as contour plots, with the contours going from 10% to 90% of the maximum height of the distribution in 10% intervals.

### 4.1. Versus RF frequency

The two tomographs compared in this subsection (figures 2(*a*) and (*b*)) were taken with the plate withdrawn. The nearest wall was 15 cm away and thus these background plasma measurements were taken in the bulk plasma, and not in the sheath or presheath. Perpendicular temperature varies significantly with RF frequency, while parallel temperature varies little. The comparison with tomographs done near the plate shows that perpendicular temperature does not change from the plasma to the presheath.

The temperatures for these distributions are best determined from the LIF scans. The equation to determine temperature (in units of energy) [17] is

$$T_\mathrm{i} = \frac{m_\mathrm{i}\lambda_0^2 \mathrm{FWHM}_\mathrm{f}^2}{8\ln 2} = m_\mathrm{i}\lambda_0^2\sigma_\mathrm{f}^2 = m_\mathrm{i}\sigma_v^2 = 4.146\times10^{-7} \times(\sigma_{v(\mathrm{m\,s^{-1}})})^2\,\mathrm{eV}, \tag{11}$$

where $T_\mathrm{i}$ is the ion temperature, $m_\mathrm{i}$ is the mass of an argon atom, $\lambda_0 = 668.61$ nm (the nominal LIF excitation wavelength), $\mathrm{FWHM_f}$ is the full-width at half-maximum of the IVDF plotted against laser frequency, $\sigma_\mathrm{f}$ is the corresponding standard deviation in frequency in Hz, and $\sigma_v$ is the standard deviation of the IVDF plotted against velocity.

In the case of bulk plasma, optical tomography reveals temperature anisotropy. Although the 2D distribution

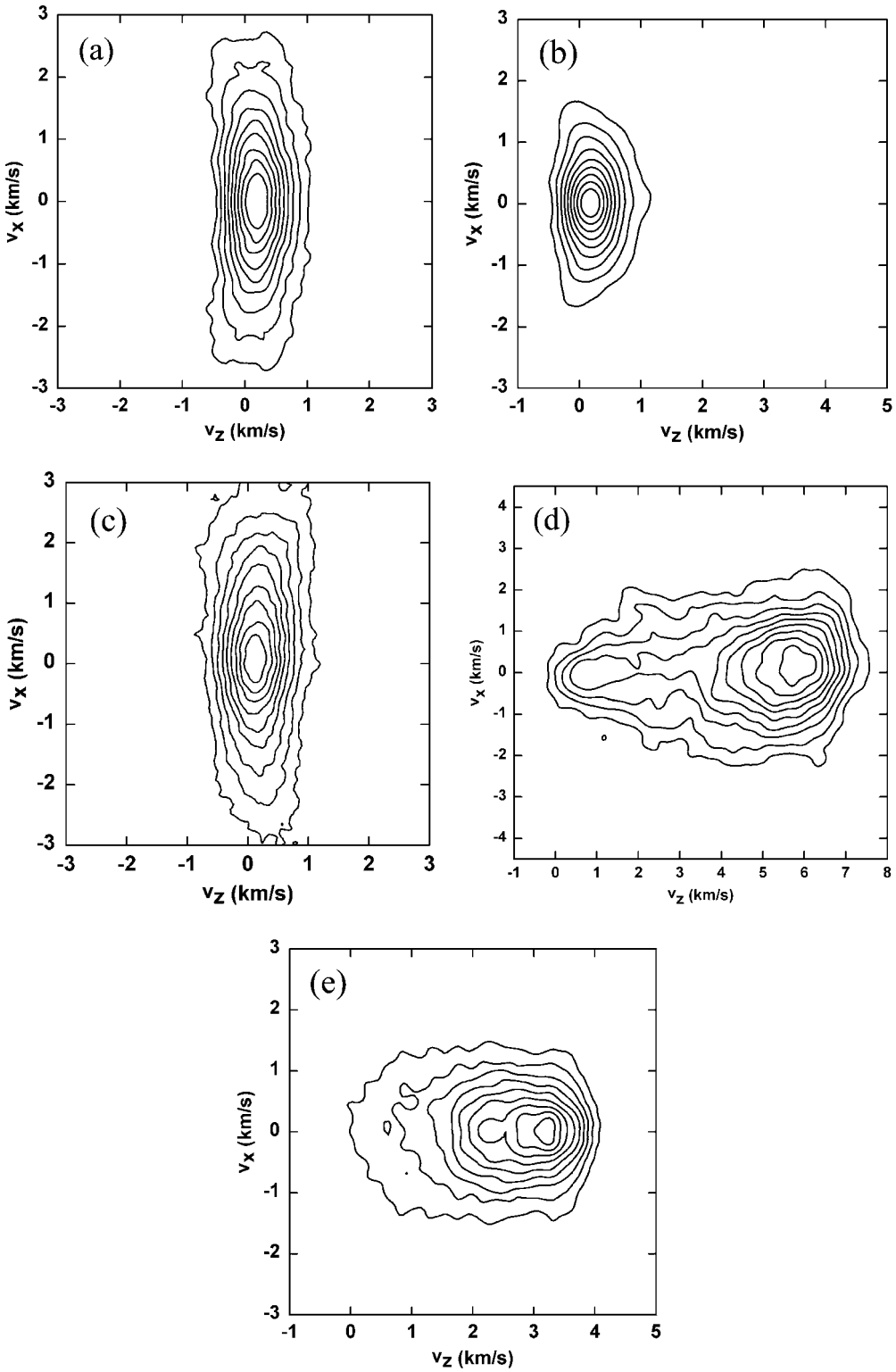


**Figure 2.** Tomographs: (*a*) 18.62 MHz bulk plasma, (*b*) 106.5 MHz bulk plasma, (*c*) 18.81 MHz, low pressure, (*d*) 18.62 MHz presheath, (*e*) 106.5 MHz presheath.

can be described well by the parallel and perpendicular LIF distributions alone, the visualization of the 2D distribution provides physical insight. Additionally, these tomographs are useful for comparison with presheath tomographs.

The perpendicular temperature (measured from the time-averaged ion velocity distribution; see section 2.2) is considerably higher at 18.62 MHz than at 106.5 MHz. To understand this, consider the azimuthal electric field induced by the changing magnetic field of the RF coil. The electric field points in the same 'direction' (clockwise or counterclockwise) about five times longer at 18.62 MHz than at 106.5 MHz. Therefore, ions are accelerated in the same

'direction' for about five times as long at 18.62 MHz. Let us eliminate the possibility of frequent ion–neutral collisions, which would nullify any differential acceleration between the two RF frequencies. The ion–neutral collision frequency is

$$\nu = \frac{v}{\lambda}, \tag{12}$$

where $\nu$ is the collision frequency, $v$ is the average ion velocity and $\lambda$ is the mean free path between collisions. Taking $v$ as the thermal velocity at a temperature of 0.9 eV and $\lambda = 6.3$ cm (see section 1), $\nu = 3 \times 10^4\ \mathrm{s}^{-1}$, hence ions undergo many RF cycles between collisions. Now, since we can assume that the plasma is collisionless over many cycles, use Newton's 2nd law to find the rms velocity:

$$F = m\frac{\mathrm{d}v}{\mathrm{d}t} = eE_0\cos(\omega t) \quad \Rightarrow \quad v_{\mathrm{rms}} = \frac{eE_0}{\sqrt{2}\omega m}, \tag{13}$$

where $m$ is the ion mass, $v$ is the ion velocity, $e$ is the electronic charge, $E_0$ is the amplitude of the rotational electric field, $\omega$ is the RF angular frequency and $v_{\mathrm{rms}}$ is the resulting rms velocity. Note that the rms velocity is inversely proportional to RF frequency, hence an effective perpendicular temperature owing to RF oscillations of ions is proportional to $\omega^{-2}$. Therefore, the perpendicular temperature of the 106.5 MHz plasma is lower than that of the 18.62 MHz plasma for a similar $E_0$. Using the measured perpendicular ion temperatures, the ratio of electric fields at the LIF measurement point can be estimated, and is

$$\frac{E_{0,106\,\mathrm{MHz}}}{E_{0,18\,\mathrm{MHz}}} = \frac{106.5\,\mathrm{MHz}}{18.62\,\mathrm{MHz}} \cdot \sqrt{\frac{T_{106\,\mathrm{MHz}}}{T_{18\,\mathrm{MHz}}}} = 3 \tag{14}$$

with $T_{106\,\mathrm{MHz}} = 0.22$ eV and $T_{18\,\mathrm{MHz}} = 0.9$ eV. The parallel temperature is also higher at lower RF frequency; this is probably due to ion–ion collisions, which would, in this case, tend to convert perpendicular energy into parallel energy in an attempt to reduce anisotropy. Using these temperatures, the rms perpendicular velocities at 18.62 MHz and 106.5 MHz RF are $1500\,\mathrm{m\,s}^{-1}$ and $730\,\mathrm{m\,s}^{-1}$, respectively, and the corresponding $E_0$ values are $1.4\,\mathrm{V\,m}^{-1}$ and $0.69\,\mathrm{V\,m}^{-1}$, respectively.

### 4.2. Versus pressure

Assuming constant gas temperature, gas density is determined by pressure. Two tomographs were taken at different pressures and similar RF frequencies to determine the effect of pressure on the velocity distribution (figures 2(*a*) and (*c*)). Again, these tomographs were taken with the plate removed.

Lowering the pressure does not significantly alter the perpendicular temperature since the ion–neutral collision frequency is already almost three orders of magnitude below the RF frequency at the higher pressure, and the pressure difference between tomographs is small. There is a small increase in temperature for the low-pressure plasma (10% increase in the perpendicular direction, 30% increase in the parallel direction). The increased temperature of the low-pressure plasma is probably due to increased RF coupling (38% more power in the low-pressure plasma), which would increase the strength of the rotational electric field.

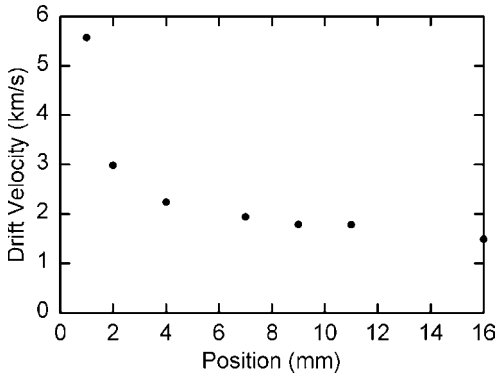


**Figure 3.** Peak ion velocity versus distance from plate.

### 4.3. Versus position

In the following discussion, all voltages are referenced to machine ground unless otherwise stated. The ions in the sheath and presheath created by a plate experience acceleration toward the grounded conducting plate. Ion drift velocity toward the plate was examined as a function of distance to a plate (figure 3). The full suite of collection optics was used to achieve spatial resolution. Under these circumstances, a region of high acceleration extends about 5 mm from the plate, with a region of low acceleration extending at least an additional 10 mm. The experimental parameters for figure 3 are: RF frequency, 95.9 MHz; radiated RF power, 6 W; gas pressure, $3.2 \times 10^{-4}$ Torr; background magnetic field at LIF point, 50 G; floating potential, about −18 V; plasma potential, about 25 V; position uncertainty, 1.5 mm.

Optical tomography was done at a point 8–10 mm from an aluminium plate (figures 2(*d*) and (*e*)), which is in the presheath of the plasma. The tomographs of the resulting IVDFs reveal features that are invisible in 1D LIF scans. Discussion as well as data pertaining to comparison of stationary plasma tomographs appear above. In this discussion, a 'cut' consists of one row or column of tomograph data whereas the discussion below involves cuts that were taken through the peaks of the presheath tomographs.

The parallel velocity spread of the plate presheath tomographs suggests that plasma was created near and away from the LIF measurement point. If no plasma was created at the measurement point, the tomograph would show a drifting distribution otherwise somewhat similar in form to that of the bulk plasma. Instead, the tomograph reveals ions drifting towards the plate with velocities between $0\,\mathrm{m\,s}^{-1}$ and the peak velocity. These slow ions may have been created just before detection at the LIF point, and therefore may not have had time to accelerate to the peak velocity before being detected. Relatively few ions are in the low velocity tail, suggesting that most of the observed ions were created in the bulk plasma.

Severn *et al* [18] observe that ions entering the sheath do so near the ion sound speed, calculated by $v_{\mathrm{s}} = \sqrt{kT_{\mathrm{e}}/m_{\mathrm{i}}}$. For a $T_{\mathrm{e}}$ of 8 eV ± 2 eV, the ion sound speed equals $4.4\,\mathrm{km\,s}^{-1} \pm 0.5\,\mathrm{km\,s}^{-1}$. The 106.5 MHz presheath plasma was moving with a peak velocity of $3.3\,\mathrm{km\,s}^{-1}$ at 74% of the ion sound speed, while the 18.62 MHz presheath plasma was moving with a peak velocity of $5.8\,\mathrm{km\,s}^{-1}$ at 132% of the ion sound speed. Overall, the measured drift velocities lie near the ion sound speed.

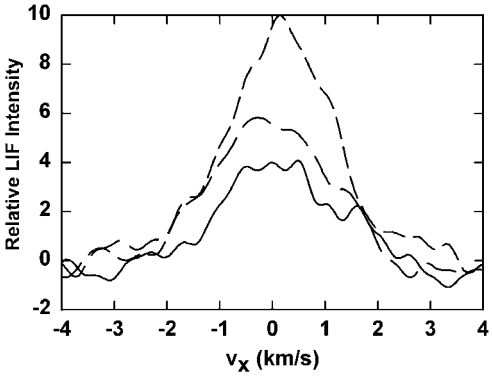


**Figure 4.** Perpendicular cuts of the 18.62 MHz presheath tomograph at different $z$ velocities. Solid line at 2 km s$^{-1}$, long dashed line at 4 km s$^{-1}$, short dashed line at 6.05 km s$^{-1}$ (peak of tomograph).

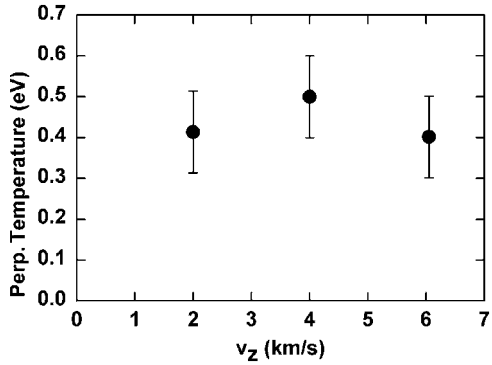


**Figure 5.** Perpendicular temperatures calculated from figure 4.

The parallel and perpendicular LIF scans are not sufficient to describe the full multidimensional velocity distribution. For example, the perpendicular temperature as a function of $v_z$ can only be determined through filtered back-projection. Figure 4 displays three perpendicular cuts of the 18.62 MHz presheath distribution at three different values of $v_z$ and figure 5 displays the corresponding temperatures. The quoted errors are those occurring for the temperature for the particular calculated cut. They underestimate the error in temperature reproducibility due to fluctuations in the LIF signal from one measurement to another and in the choice of cutoff speeds for temperature calculations, as can be seen by the two calculated temperatures at 4 km s$^{-1}$, one being calculated from the entire cut, the other from the data obtained between $-2$ km s$^{-1}$ and +2 km s$^{-1}$ only. The greater error of about $\pm 0.1$ eV comes from the noise in the LIF data and the process of tomographic reconstruction.

## 5. Ion beam results and discussion

The attempt at performing optical tomography on the ion beam source IVDF was not successful. The energy of the beam ions from the ion beam source varies by as much as 20 eV when maintaining the screen and accelerator voltages constant (figure 6). The beam energy is not a function of pressure, which was the variable parameter for display in figure 6. We have not found a pressure-dependent fit that falls within all error bars. If an attempt were made to recreate these data, different beam energies would exist for the same parameter

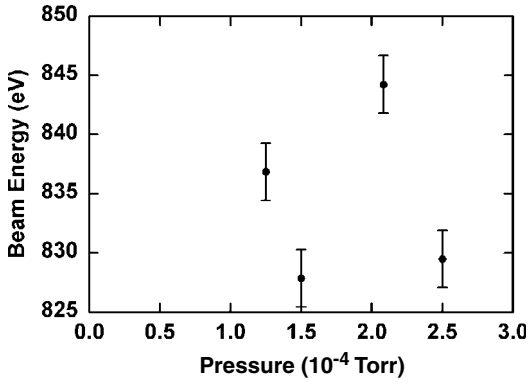


**Figure 6.** Random variation of beam energy versus pressure.

sets, with these energies changing in time over a timescale of a few minutes. The cause of the observed energy fluctuation remains unknown at this time. The power supplies controlling the screen and accelerator voltages have a measured drift in a range of approximately $\pm 2.5$ V about the set point. However, these drifts cannot account for the full drift in beam energy. There exists a possibility that the plasma potential inside the ion beam source varies owing to changing internal wall and RF coupling conditions. In any case, one or more unknown parameters are the cause of an energy fluctuation greater than the energy spread of the beam, making optical tomography impossible. Obtaining single LIF scans within a time period where the beam energy was not changing (i.e. it sits at a steady beam energy for a few minutes and then jumps) has been proven possible. Under this type of scan arrangement, we were able to measure the parallel IVDF as a function of screen voltage. These 1D scan results have been reported in [15]. Although we failed to collect valid tomographic data, our progress is important because we have discovered problems for future researchers to solve.

## 6. Conclusions

The 2D ion velocity distribution of inductively coupled RF plasma has been measured in the bulk plasma and in the presheath of a plate with LIF and optical tomography. The resulting tomographs display pronounced temperature anisotropy and, in the case of the presheath plasma, a drift of up to 7 km s$^{-1}$ toward the plate. Ion temperature depends on RF frequency and is weakly dependent on pressure.

The characteristics of a modified commercial ion beam source have been explored with LIF. Ion beam energy is higher than the accelerating voltage by an offset of $\sim$100 eV. This offset fluctuates in a matter of minutes by up to 20 eV, which hampers LIF measurements and makes tomography measurements impossible, in addition to altering the ion beam energy. The dependence of the offset fluctuation on experimental parameters is unknown.

## Acknowledgments

The authors wish to thank the NSF (INT-9981978), the US DoE (DE-FG03-00ER54587) and Lam Research Inc. for funding related to the paper presented here.

## References


[1] Koslover R A and McWilliams R 1986 Measurement of multidimensional ion velocity distributions by optical tomography *Rev. Sci. Instrum.* **57** 2441

[2] Zintl M, McWilliams R and Wolf N S 1995 Transverse ion acceleration and ion conic formation in a divergent-field laboratory plasma *Phys. Plasmas* **2** 4432

[3] Sheehan D P, Koslover R and McWilliams R 1991 Laboratory simulations of suprauroral mechanisms leading to perpendicular ion heating & conic formation *J. Geophys. Res.* **96** 14107

[4] Zintl M W and McWilliams R 1994 Improved optical tomography device *Rev. Sci. Instrum.* **65** 2574

[5] Scime E E *et al* 2000 Ion temperature anisotropy limitation in high beta plasmas *Phys. Plasmas* **7** 2157

[6] Biloiu C *et al* 2004 Scanning internal probe for plasma particle, fluctuation, and LIF tomographic measurements *Rev. Sci. Instrum.* **75** 4296

[7] Severn G D, Edrich D A and McWilliams R 1998 Argon ion laser-induced fluorescence with diode lasers *Rev. Sci. Instrum.* **69** 10

[8] Edrich D A, McWilliams R and Wolf N S 1996 Single beam laser induced fluorescence technique for plasma transport measurements *Rev. Sci. Instrum.* **67** 2812

[9] Sadeghi N *et al* 1991 Ion transport in an electron cyclotron resonance plasma *J. Appl. Phys.* **70** 2552

[10] Giapis K P *et al* 1993 Limits to ion energy control in high density glow discharges: measurement of absolute metastable ion concentrations *J. Appl. Phys.* **73** 7188

[11] Brockhaus A, Yuan Y and Engemann J 1995 Determination of the ion velocity in a radio frequency ion beam by laser-induced fluorescence *J. Vac. Sci. Technol.* A **13** 400

[12] Wobschall D, Graham J R Jr and Malone D P 1963 Ion cyclotron resonance and the determination of collision cross sections *Phys. Rev.* **131** 1565

[13] Lieberman M A and Lichtenberg A J 1994 *Priciples of Plasma Discharges and Materials Processing* (New York: Wiley)

[14] Hershkowitz N 1994 How does the potential get from A to B in a plasma? *IEEE Trans. Plasma Sci.* **22** 11

[15] Boehmer H *et al* 2004 Operation of a 0.2–1.1 keV ion source within a magnetized laboratory plasma *Rev. Sci. Instrum.* **75** 1013

[16] Gerstenkorn S and Luc P 1978 *Atlas du Spectre D'absorption De La Molucule D'iode* (Paris: Editions Du Centre National De La Recherche Scientifique)

[17] Goeckner M J and Goree J 1989 Laser-induced fluorescence measurement of plasma ion temperatures: corrections for power saturation *J. Vac. Sci. Technol.* A **7** 977

[18] Severn G D *et al* 2003 Experimental studies of the Bohm criterion in a two-ion-species plasma using laser-induced fluorescence *Phys. Rev. Lett.* **90** 145001